Title
Inhibition of BTK and PI3Kδ impairs the development of human JMML stem and progenitor cells

Journal
Molecular Therapy, 30(7)

ISSN
1525-0016

Authors
Ramdas, Baskar
Yuen, Lisa Deng
Palam, Lakshmi Reddy
et al.

Publication Date
2022-07-01

DOI
10.1016/j.ymthe.2022.04.009

Peer reviewed

Molecular Therapy
Original Article

Inhibition of BTK and PI3Kδ impairs the development of human JMML stem and progenitor cells

Baskar Ramdas,[1,10] Lisa Deng Yuen,[1,2,10] Lakshmi Reddy Palam,[1] Roshini Patel,[1] Santhosh Kumar Pasupuleti,[1] Victoria Jideonwo,[1] Ji Zhang,[1] Callista Maguire,[3] Eric Wong,[4] Rahul Kanumuri,[1] Chujing Zhang,[4] George Sandusky,[3] Rebecca J. Chan,[5] Chi Zhang,[6] Elliot Stieglitz,[4,7] Laura Haneline,[1] and Reuben Kapur[1,6,8,9]

[1]Department of Pediatrics, Herman B Wells Center for Pediatric Research, Indiana University School of Medicine, Indianapolis, IN, USA; [2]Department of Pathology, Massachusetts General Hospital, Boston, MA, USA; [3]Department of Pathology, Indiana University School of Medicine, Indianapolis, IN, USA; [4]Department of Pediatrics, Benioff Children's Hospital, University of California, San Francisco, CA, USA; [5]Senior Director, Oncology, U.S. Medical Affairs, Gilead Sciences, Inc., 333 Lakeside Drive, Foster City, CA, USA; [6]Department of Medical and Molecular Genetics, Indiana University School of Medicine, Indianapolis, IN, USA; [7]Helen Diller Family Comprehensive Cancer Center, University of California, San Francisco, CA, USA; [8]Department of Microbiology and Immunology, Indiana University School of Medicine, Indianapolis, IN, USA; [9]Department of Molecular Biology and Biochemistry, Indiana University School of Medicine, Indianapolis, IN, USA

Juvenile myelomonocytic leukemia (JMML) is an aggressive myeloproliferative neoplasia that lacks effective targeted chemotherapies. Clinically, JMML manifests as monocytic leukocytosis, splenomegaly with consequential thrombocytopenia. Most commonly, patients have gain-of-function (GOF) oncogenic mutations in *PTPN11* (SHP2), leading to Erk and Akt hyperactivation. Mechanism(s) involved in co-regulation of Erk and Akt in the context of GOF SHP2 are poorly understood. Here, we show that Bruton's tyrosine kinase (BTK) is hyperphosphorylated in GOF Shp2-bearing cells and utilizes B cell adaptor for PI3K to cooperate with p110δ, the catalytic subunit of PI3K. Dual inhibition of BTK and p110δ reduces the activation of both Erk and Akt. *In vivo*, individual targeting of BTK or p110δ in a mouse model of human JMML equally reduces monocytosis and splenomegaly; however, the combined treatment results in a more robust inhibition and uniquely rescues anemia and thrombocytopenia. RNA-seq analysis of drug-treated mice showed a profound reduction in the expression of genes associated with leukemic cell migration and inflammation, leading to correction in the infiltration of leukemic cells in the lung, liver, and spleen. Remarkably, in a patient derived xenograft model of JMML, leukemia-initiating stem and progenitor cells were potently inhibited in response to the dual drug treatment.

INTRODUCTION

Juvenile myelomonocytic leukemia (JMML) is the most common myeloproliferative neoplasm (MPN) in childhood and tends to occur in children less than 4 years of age. JMML is characterized as being Ras-driven due to mutations in *NF1*, *CBL*, *KRAS, NRAS*, or *PTPN11*,[1] and cells demonstrate hypersensitivity to the cytokine GM-CSF.[2] Traditional cytotoxic chemotherapy agents are ineffective in JMML, and the only curative modality is allogeneic hematopoietic stem cell transplantation (HSCT).[3,4] However, even with this therapy, approximately 50% of patients relapse, and a second transplant only rescues a third of patients.[4–7] Somatic activating mutations in *PTPN11*, which encodes the protein tyrosine phosphatase, SHP2, are the most common cause of JMML and lead to hyperactive Ras signaling.[8–11]

Targeting the gain-of-function (GOF) mutant SHP2 as a treatment strategy for JMML has been largely unsuccessful, although an allosteric inhibitor of wild-type (WT) SHP2 protein, SHP099, has shown promise for treatment of acute myeloid leukemia (AML).[12,13] However, SHP099 does not inhibit the activity of GOF SHP2.[12] Thus, a significant focus has been placed on identifying downstream kinases from GOF SHP2 that could potentially be targeted for therapeutic purposes. In this context, putative targets would be those with a restricted expression profile (i.e., hematopoietic specific to minimize toxicity to other tissues), preferably targets for which drugs have already been FDA approved for other disease indications in order to expedite clinical utility as well as those that can be efficacious when given in combination with another drug to avoid drug resistance as is often seen with a single therapeutic agent.

We have previously shown that p110δ, the hematopoietic-specific catalytic subunit of phosphoinositide 3-kinase (PI3K), is activated

Received 25 March 2022; accepted 16 April 2022;
https://doi.org/10.1016/j.ymthe.2022.04.009.

[10]These authors contributed equally

Correspondence: Ramdas Baskar, PhD, Assistant Research Professor of Pediatrics, Indiana University School of Medicine, Indianapolis, IN 46202, USA.
E-mail: ramdasb@iu.edu
Correspondence: Reuben Kapur, PhD, Professor of Pediatrics, Herman B Wells Center for Pediatric Research, Indiana University School of Medicine, 1044 W. Walnut Street, R4-168, Indianapolis, IN 46202, USA.
E-mail: rkapur@iu.edu

by Shp2 GOF mutation.[14] However, the mechanism(s) that fully activate the PI3K signaling in Shp2 GOF mutant-bearing cells are still poorly understood. Furthermore, it is unclear if p110δ alone contributes to GM-CSF hypersensitivity or if it interacts with other signaling molecules to promote aberrant Shp2 signaling in myeloid cells. In recent years, a key player in B cell receptor (BCR) signaling, Bruton's tyrosine kinase (BTK), has been extensively studied in lymphoid malignancies. Ibrutinib, a small molecule inhibitor targeting BTK, has proven to be effective and has received FDA approval for the treatment of a variety of B cell malignancies.[15] Although research on BTK has primarily focused on B cell malignancies, BTK is also highly expressed in myeloid cells.[16,17] Thus, it is possible that BTK signaling may also play an important role in myeloid malignancies, such as JMML. Given the interplay of BTK and p110δ in BCR signaling and the high expression of BTK in myeloid cells, we hypothesized that BTK and p110δ function together in GOF Shp2-expressing myeloid cells to promote MPN. We found that BTK phosphorylates B cell adaptor for PI3K (BCAP) in response to GM-CSF in GOF Shp2-expressing myeloid cells and facilitates the activation of Akt via the canonical PI3K/Akt pathway, as well as Erk activation by cross-talk between signaling pathways. We also examined the potential collaboration of BTK and p110δ in GOF Shp2-expressing mice using single and combined drug treatments *in vivo* to test their impact on gene expression and leukemia phenotypes. We found individual drug treatment in a mouse model of human JMML reduces monocytosis and splenomegaly, but combined drug treatment uniquely rescues thrombocytopenia. In a patient-derived xenograft (PDX) model of JMML, we show that the combined drug treatment profoundly impairs the growth and survival of human leukemia initiating cells. We further provide molecular mechanism(s) by which these drugs function in JMML. Our findings support the use of BTK inhibitor alone or in combination with p110δ inhibitor in treating human JMML.

RESULTS

Dual inhibition of BTK and PI3K-p110δ efficiently inhibits Akt and Erk phosphorylation in GOF *Shp2*$^{E76K/+}$ mutation-expressing myeloid cells

We have recently shown that PI3K catalytic subunit p110δ partly contributes to both Akt and Erk hyperactivation and promotes Shp2-induced GM-CSF hypersensitivity in GOF Shp2-bearing myeloid cells.[14] Given the lack of complete correction of hyperactive Akt and Erk in the absence of p110δ in Shp2 GOF-bearing myeloid cells, we sought out putative tyrosine kinases that signal together with p110δ in the PI3K-Akt signaling pathway that could be targeted in JMML.

In the B cell canonical pathway, BTK is recruited by its Pleckstrin homology domain to the membrane via PI (3,4,5) P_3, the phosphorylated lipid product of PI3K and signals to PLCγ2 and PKC to activate Erk and induce proliferation. Given the known expression of BTK in myeloid cells,[18] we speculated that BTK may be a rational target collaborating with PI3K p110δ in GOF Shp2-expressing cells. Stimulation of GOF Shp2-bearing cells with GM-CSF resulted in BTK and PLCγ2 hyperphosphorylation both at baseline and after stimulation with GM-CSF (Figure S1), indicating that BTK function is upregulated in GOF Shp2 cells, and suggesting that this may play an important role in proliferative signaling.

To investigate how BTK and p110δ cooperate in *Ptpn11*$^{E76K/+}$ mutant-expressing myeloid cells, we examined phospho-BTK, phospho-Akt, and phospho-Erk levels. We also examined the levels of phospho-PLCγ2 at two tyrosine sites that have been shown to be phosphorylated by BTK (Y759 and Y1217).[19–21] Bone marrow (BM)-derived *Ptpn11*$^{E76K/+}$ myeloid cells were starved followed by GM-CSF stimulation with or without BTK and p110δ inhibitors. Phospho-BTK was predictably decreased in a dose-dependent manner in the presence of BTK inhibitor, and it was also decreased by p110δ inhibition, indicating that BTK is downstream of p110δ in *Ptpn11*$^{E76K/+}$-expressing myeloid cells (Figure S1; lanes 3 to 6). However, in contrast to earlier reports involving B cell signaling, PLCγ2 phosphorylation was unchanged by either inhibitor, suggesting that PLCγ2 might not be regulated by BTK or p110δ in GOF Shp2-expressing myeloid cells. We next examined the effect of drug treatment on Erk and Akt activation in these cells. We observed a decrease in phospho-Akt and phospho-Erk activation in the presence of ACP-196 and ACP-319 (Figure 1A). We also observed a further reduction in phospho-Akt and phospho-Erk levels in cells treated with the combination of two drugs (Figure 1A; lanes 6 and 7). These data suggest that BTK cooperates with p110δ in signaling to Akt and Erk activation in GOF Shp2-expressing myeloid cells, and that this occurs independent of PLCγ2, even though PLCγ2 is hyperphosphorylated by *Ptpn11* in myeloid cells. Thus, in myeloid cells expressing GOF Shp2, there is more phospho-BTK, and a p110δ inhibitor decreases this phosphorylation, indicating that this part of the signaling pathway is conserved in B cells and myeloid cells. However, in myeloid cells, BTK does not signal through PLCγ2 to affect Erk activation. We therefore speculated that B cell adaptor for PI3K (BCAP), which was first described as a BTK substrate that activates PI3K in the context of BCR signaling,[22] could be a downstream target of BTK in JMML.

BCAP has been studied in normal B cell signaling and is known to be directly phosphorylated and activated by BTK.[22] Once phosphorylated, BCAP binds to PI3K at the regulatory p85α subunit of PI3K. This interaction promotes the activity of the catalytic subunit of PI3K and recruits PI3K to the plasma membrane where it can better access its substrate. These two methods by which BCAP activates PI3K lead to the formation of a positive feedback loop with BTK. We next wondered if BCAP could be the molecule responsible for connecting BTK to Akt and Erk activation in GOF Shp2-expressing myeloid cells. Because of alternative splicing, BCAP is expressed as a full-length and a short form and due to posttranslational modifications, these transcripts produce isoforms of four different sizes.[22] Both the full-length and short transcripts have three YxxM motifs. When these tyrosines become phosphorylated, the phospho-YxxM motifs can bind to p85α. We first assessed if Shp2 mutant cells would have more phospho-BCAP. We immunoprecipitated BCAP and

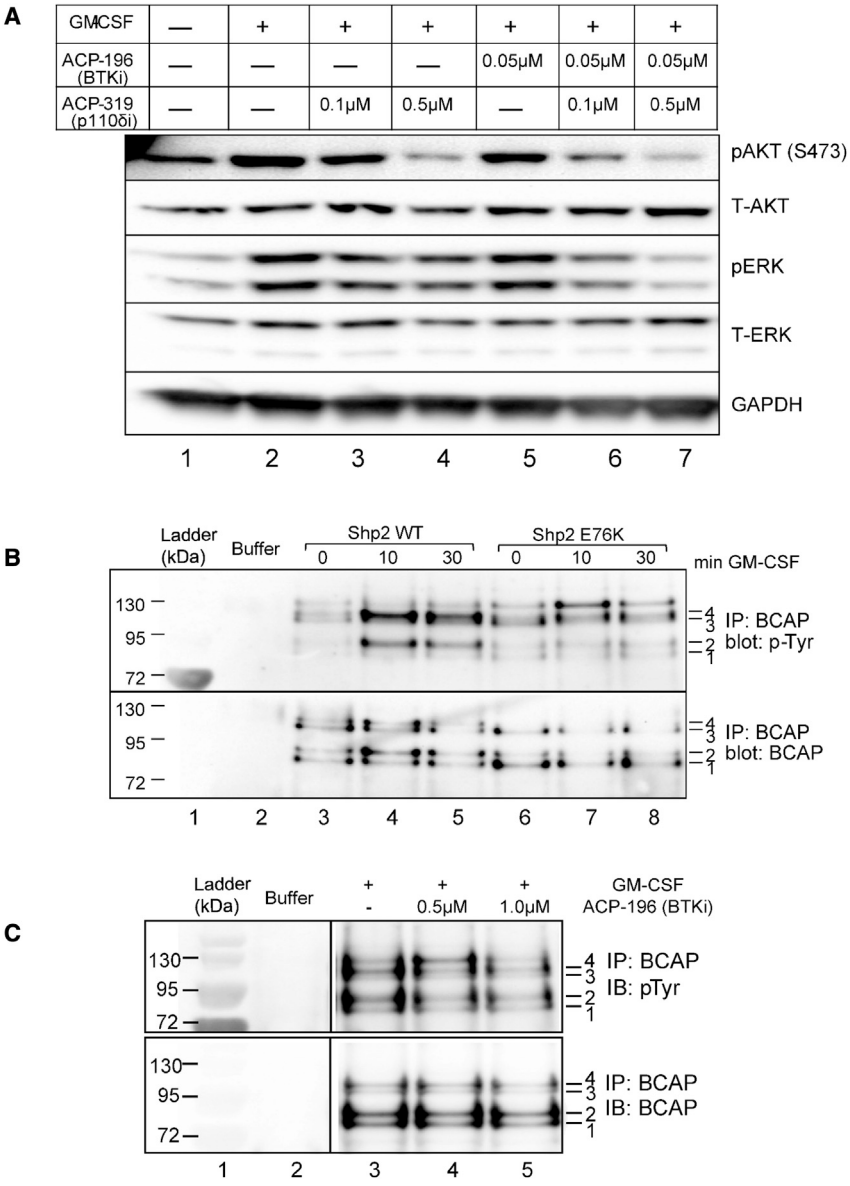

Figure 1. Dual inhibition of BTK and PI3K-p110δ efficiently inhibits Akt and Erk phosphorylation in GOF *Shp2*$^{E76K/+}$ mutation-expressing myeloid cells

(A) BM-derived myeloid cells from WT and GOF *Shp2*$^{E76K/+}$ mice were treated for 1 h with increasing concentrations of BTK inhibitor along with the PI3K-p110δ inhibitor in the presence of GM-CSF (10 ng/mL). Western blot analysis was performed using an anti-pAkt or an anti-pErk antibody. Shown are the levels of active and total Akt and Erk. (B) Protein lysates from (A) were subjected to immunoprecipitation with an anti-BCAP antibody and immunoblotted with an anti-phosphotyrosine antibody. 1 and 2 indicate the truncated isoforms of BCAP; 3 and 4 indicate the full-length isoforms. (C) BCAP phosphorylation was reduced by BTK inhibitor in a dose-dependent manner in GOF *Shp2*$^{E76K/+}$-bearing myeloid cells.

blotted with anti-phospho-tyrosine antibody. We observed four isoforms of BCAP as reported. In WT myeloid cells, there was increased phosphorylation of two of the four isoforms (Figure 1B, lanes 3–5). However, we saw a different pattern of BCAP phosphorylation in Shp2 mutant cells. There was increased phosphorylation specifically of the full-length BCAP isoform (Figure 1B, lanes 6–8). This has important implications for PI3K activation. A study by Ni et al.[23] involving Syk knockout myeloid cells revealed increased BCAP phosphorylation specifically in the larger two isoforms, which was associated with more interaction with p85α, suggesting that the larger isoforms of full-length BCAP are more important for binding to p85α than the smaller isoforms. To confirm the involvement of BTK in the phosphorylation of BCAP in myeloid cells, we treated the GOF Shp2-expressing cells with the BTK inhibitor, ACP-196 (acalabrutinib), then pulled down total BCAP and probed with p-tyrosine antibody. We found that the BTK inhibitor treatment reduced the phosphorylation of BCAP in a dose-dependent manner, indicating that BTK does signal to BCAP in GOF Shp2-bearing myeloid cells (Figure 1C).

Individual and combined inhibition of BTK and/or PI3K-p110δ reduces splenomegaly observed in *Shp2*$^{E76K/+}$ mice

To validate the *in vitro* findings related to the impact of BTK inhibitor, *in vivo*, in a murine model of JMML, we used GOF *Shp2*$^{E76K/+}$ mice. 15- to 20-week-old male and female GOF *Shp2*$^{E76K/+}$ mice were treated with 20 mg/kg bw of BTK inhibitor (BTKi; acalabrutinib, ACP-196) and/or PI3K-p110δ inhibitor (ACP-319) individually or in combination, twice a day for 3 weeks. Mice were sacrificed at 3 weeks and subjected to complete hematopoietic analysis (Figure 2A). Monocytosis is one of the cardinal features of JMML. We noted a significant correction in the elevated monocyte counts including the presence of CD11b-positive mutant myeloid cells in the peripheral blood (PB) of Shp2$^{E76K/+}$ mice in all three drug treatment groups (Figure 2B (i) (ii)). As splenomegaly is another hallmark feature of JMML, we next examined the impact of the two drugs on splenomegaly in GOF Shp2$^{E76K/+}$ mice. Both drugs were equally potent at correcting splenomegaly in the Shp2$^{E76K/+}$ mice (Figure 2C (i) and (ii)), as well as in reducing the burden of mutant myeloid cells as determined by flow cytometry analysis of CD11b- and Gr-1-positive mature cells (Figure 2C (iii)). A greater reduction in the frequency of splenic Gr1/CD11b double-positive leukemic myeloid cells was noted in mice treated with the combination of two drugs (Figure 2C (iv)). Overall, these data suggest that individual and combined drug treatment reduced some of the cardinal pathologies associated with JMML.

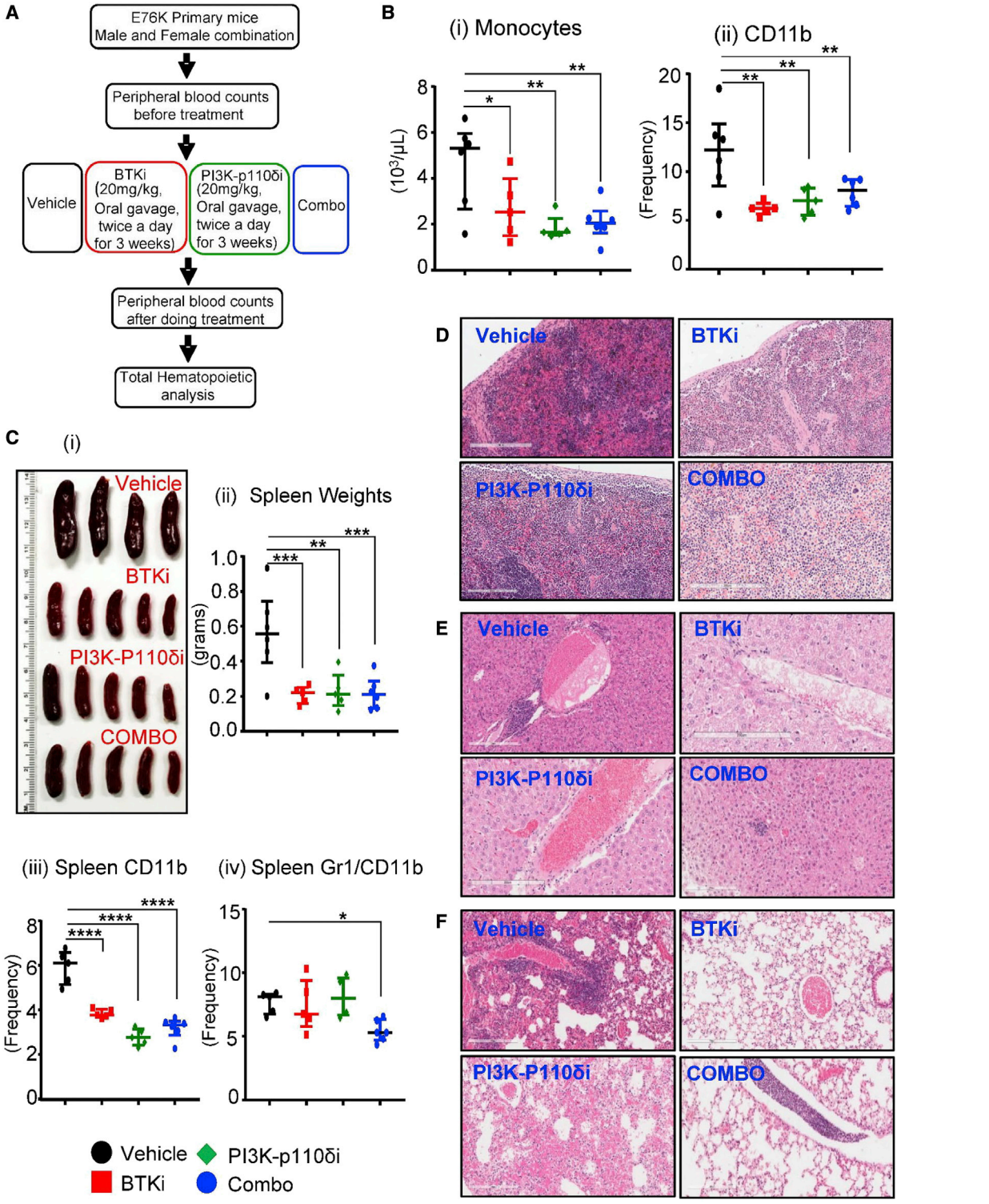

(legend on next page)

Combination of BTK and PI3K-p110δ inhibitor restores normal splenic architecture and reduces focal leukemic cells and lung invasiveness in GOF *Shp2*$^{E76K/+}$ mice

Given the most profound symptoms seen in patients with JMML include splenomegaly, hepatomegaly, and myeloid cell infiltration in the lung, we assessed the impact of BTK and p110δ inhibitors alone or in combination on GOF Shp2$^{E76K/+}$ mice for the infiltration of leukemic cells in various tissues. As shown earlier, a significant normalization in the spleen size and weight was observed when GOF *Shp2*$^{E76K/+}$ mice were treated with either one of the drugs. In the vehicle-treated group, as the disease progresses, the germinal center coalesces as the leukemic cells proliferate, and the spleen becomes denser, as seen in Figure 2D (vehicle group). Figure 2D shows a side-by-side comparison between the spleens recovering from an overgrowth of leukemic cells in the subcapsular zone across the four treatment groups. In addition, we observed the presence of greater numbers of megakaryocytes in mice treated with the combination of two drugs. In the liver, we not only observed leukemic cells distributed throughout the parenchyma in the vehicle group, but also progression of leukemia in a perivascular pattern (Figure 2E). The decrease in focal leukemia in the drug combination treatment group compared to the severity seen in the vehicle control liver is noticeable. In the lung, we observed leukemic infiltration, most extensive in the vehicle-treated group (Figure 2F). Only focal invasiveness is observed in the BTK and combination drug-treated mice. In contrast, p110δ inhibitor-treated mice had lungs without leukemia involvement (Figure 2F). Consistent with the data presented in Figure 2C, histopathology analysis correlates with the restoration of normal splenic germinal center architecture and reduction of focal leukemic cells and lung invasiveness.

RNA-seq analysis revealed significant modulation in the expression of genes associated with leukemic cell migration and motility in response to dual drug treatment in GOF *Shp2*$^{E76K/+}$ mice

To assess the impact of drugs on the expression of genes in *Shp2*$^{E76K/+}$ mice, we performed RNA-seq analysis. Differentially expressed genes were assessed in the scatterplot analysis (SPA) (Figure 3A). Gene expression changes with a p value < 0.01 and >1.5 or < –1.5-fold change were considered for SPA (Figure 3A). The lower left quadrant represents a large number of genes that are downregulated in *Shp2*$^{E76K/+}$ mice treated with either the BTK or the PI3K-p110δ inhibitor. This includes genes involved in processes such as the cell cycle (*Lats1,*[24] *Dvl3*), leukocyte signaling (*Cxcr2*),[25] cytokine stimulation (*Socs4*),[26] and stem cell activation (*Hdac4*).[27] As seen in the top-left quadrant, only a few genes are uniquely upregulated in response to only PI3K-p110δ inhibitor treatment but downregulated in response to BTK inhibitor treatment. The top-right quadrant in the SPA represents genes that are upregulated in either PI3K-p110δ inhibitor or the BTK inhibitor treatment conditions. This includes membrane-related genes such as *cadherin 2 (Cdh2)*[28] and *claudin 5 (Cldn5)* (Figure 3A). In contrast, the bottom-right quadrant shows genes that are uniquely upregulated by the BTK inhibitor treatment but downregulated in response to the PI3K-p110δ inhibitor treatment. This quadrant includes genes involved in the regulation of the cell cycle such as the *ets* transcription factor *Elk4,*[29] mitogen-activated protein kinase kinase kinase 13 (*Map3k13*)[30] and cyclin-dependent kinase 15 (*Cdk15*).[31]

In addition to the SPA, we also conducted IPA analysis. Among many affected pathways, activation of mTOR signaling and downstream eIF4 and p70S6K signaling was repressed, which is consistent with the reduced pAkt levels observed in mice treated with the p110δ inhibitor (Figures S2 and 1A). Additionally, IPA analysis revealed that the dual drug treatment led to a significant decrease in the expression of genes involved in inflammation (Figure 3B). Consistent with these findings, *Irf7* (interferon regulatory factor 7),[32] a key transcriptional regulator of type I interferon (IFN)-dependent immune response, was significantly repressed in mutant cells treated with a combination of the two drugs (Figure 3C). Consistent with the observations made utilizing IPA, GSEA also revealed that GOF *Shp2*$^{E76K/+}$ mice treated with the dual drug combination resulted in decreased PI3Kinase signaling (NES: −1.99, $p < 0.001$), inositol phosphate metabolism (NES: −1.92, $p < 0.001$), BCR signaling pathway (NES: −1.67, $p < 0.001$), extracellular matrix interaction (NES: −2.17, $p < 0.001$), focal adhesion (NES: −2.02, $p < 0.001$), and actin cytoskeleton regulation (NES: −1.73, $p < 0.001$) (Figure 3D). We hypothesized that drug treatment might modulate the genes involved in motility, migration, and extravasation in GOF *Shp2*$^{E76K/+}$ mice. The expression of genes involved in cell motility, migration, and extravasation was profoundly impacted in GOF *Shp2*$^{E76K/+}$ mice treated with these two drugs. The expression of Snail family transcriptional repressor 1 (*Snail1*), which is involved in epithelial to mesenchymal transition, mesoderm formation, cell growth, survival, and migration, and known to bind to E-cadherin/CDH1 promoter was reduced in all the three drug treatment groups (Figures 3C and 3E).[33] Likewise, Ras homology family V (*RhoV*) was significantly downregulated in mice treated with the two drugs (Figures 3C and 3E). RhoV is involved in Rho GTPase signaling and GPCR signaling and is an important paralog of RHOU (Ras homolog family member U), which is involved in PAK1 and JNK1 activation and mediates

Figure 2. Combination of BTK and PI3K-p110δ inhibitor restores germinal center and reduces focal leukemic cells and lung invasiveness in GOF Shp2$^{E76K/+}$ mice

(A) Schematic of experimental design. (B) (i) PB monocyte counts. (ii) Frequency of PB CD11b cells. (C) (i) Image showing reduction in splenomegaly upon drug treatment. (ii) Spleen weights. (iii) Spleen CD11b+ cells and (iv) spleen Gr1/CD11b+ cells. Histopathologic features of spleen, liver, and lungs, respectively (D), (E), and (F). Representative H&E stained images from vehicle- and drug-treated groups. All images were acquired at 20x, with the 200-μm scale bar. Median values for each group are shown with interquartile range. Statistical analysis was performed using GraphPad version 7 by one-way ANOVA with uncorrected Fisher's test. *$p < 0.05$, **$p < 0.01$, ***$p < 0.001$, ****$p < 0.0001$.

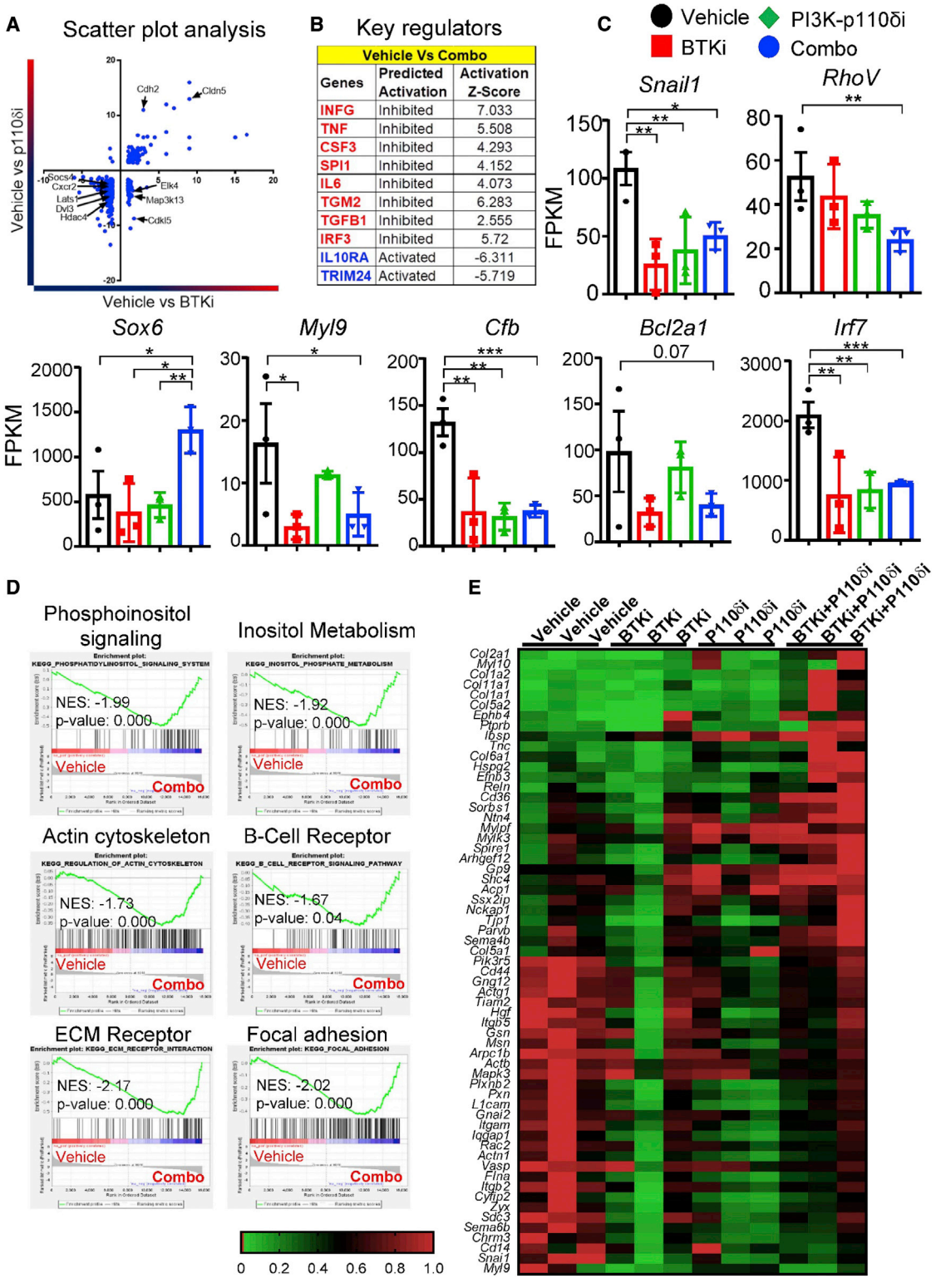

(legend on next page)

filopodia formation and stress fiber dissolution.[34] Furthermore, GSEA analysis and IPA analysis support our biochemical data demonstrating that dual inhibitor treatment significantly blocks the Akt and Erk signaling and thus represses cell proliferation by decreasing the expression of genes involved in proliferation such as *Cfb* (compliment factor B),[35] *Bcl2a1* (anti-apoptotic factor),[36] and cell cycle progression genes such as *elk4*[29] and *cdkl5*[31] (Figures 3A and 3C). Sex determining region Y-box 6 (*Sox6*) expression was enhanced in drug-treated mice (Figure 3C). *SOX6* is involved in deactivation of β-catenin transactivating complex and in cell migration and invasiveness.[37]

Individual and combined inhibition of BTK and/or PI3K-p110δ rescues erythroid and megakaryocyte deficiencies in GOF Shp2$^{E76K/+}$ mice

Clinically, in addition to monocytosis and splenomegaly, JMML patients suffer from anemia and thrombocytopenia. We next asked if BTK and p110δ are also involved in regulating the above two outcomes due to the presence of GOF Shp2. As seen in Figures 4A–4C, BTK and PI3K-p110δ inhibitors alone as well as in combination rescued various peripheral erythroid cell abnormalities associated with JMML including correction in anemia with improved peripheral RBC counts, hemoglobin (Hb) levels, and hematocrits (HCTs) into the normal reference range. Inhibition of either BTK alone or the p110δ alone was sufficient to achieve these corrections. While not always statistically different, the rescue in the peripheral erythroid parameters was more robust in mice treated with the combination of two drugs (Figures 4A–4C). Remarkably, these drugs also led to the correction of thrombocytopenia, with a more significant correction seen in mice treated with the combination of two drugs (Figure 4D). We next searched for genes involved in the rescue of erythroid cells and megakaryocytes upon drug treatment. We interrogated genes involved in erythroid/megakaryocyte development and growth and found a significant increase in the expression of genes that promote the growth and differentiation of these two lineages (Figure 4E). Genes involved in the maturation of fully differentiated erythroid and megakaryocytic cells including *Klf1, EpoR, Gata1, Hemgn, CD56b*, *CD36*, and *Add2* were all upregulated in drug-treated mice, with the most changes noted in mice treated with the combination of the two drugs (Figures 4E and 4F). In contrast, B cell signaling-related gene expression was repressed in the presence of either drug treatment, which is consistent with a known role for BTK and p110δ in B cell development (Figure 4E).

Impact of single and/or combined drug treatment on stem and progenitor cells bearing GOF *Shp2*$^{E76K/+}$ mutation

To determine how the treatment of GOF *Shp2*$^{E76K/+}$ mice with BTK and/or p110δ inhibitor impacts the development of relatively immature cells in the BM, we performed flow cytometry analysis on BM cells. As seen in the Figure 5A, the elevated frequency of stem cells containing lineage negative Sca1^{Pos} Kit^{Pos} (LSK) population of the BM was significantly reduced in response to either drug treatment as well as in response to the combination of two drugs. Figure 5C shows representative flow profiles of LSK cells derived from various drug treatment groups. Given that LSK cells are a heterogeneous population, we further assessed LSK cells for the proportion of hematopoietic progenitor-1 (HPC1) (LSK CD150^{Neg}, CD48^{Pos}) cells, which define a more immature phenotype compared to LSK cells. As seen in Figure 5B, the frequency of HPC1 cells was significantly reduced in both single-drug treatment groups; however, the inhibition was most dramatic in mice treated with a combination of the two drugs. Lower panels in Figure 5C show representative flow profiles of HSC and HPC1 cells within the LSK fraction of the BM. To evaluate the impact of drug treatment on committed progenitors, we assessed the frequencies of common myeloid progenitors (CMPs), granulocyte macrophage progenitors (GMPs), and megakaryocyte erythroid progenitors (MEPs) in various drug treatment groups. Interestingly, both drugs enhanced the frequency of CMPs while reduced the frequency of GMPs in the BM (Figures 5D and 5E). Importantly and consistent with the PB platelet counts as shown in Figure 4D, the frequency of megakaryocytes in the BM was significantly more in GOF *Shp2*$^{E76K/+}$-treated mice with a combination of the two drugs (Figure 5F). To assess whether the impact of drug treatment on committed myeloid progenitors impacts their more mature downstream progeny, we examined CD11b cells in the BM. As seen in Figure 5G, the frequency of CD11b cells was significantly reduced in GOF *Shp2*$^{E76K/+}$ mice treated with a combination of both BTK and PI3K-p110δ inhibitor. Taken together, these data suggest that individual drug treatment reduced the frequency of primitive GOF *Shp2*$^{E76K/+}$-bearing cells, while the combination drug treatment uniquely inhibits both more primitive cells as well as immature myeloid CD11b-positive cells.

Next, to gain a deeper insight into the impact of BTK and p110δ inhibition on the differentiation of committed progenitors, we further assessed the CMP population. Combined inhibition of BTK and

Figure 3. RNA-seq analysis revealed significant modulation in the expression of genes associated with leukemic cell migration and motility in response to dual drug treatment in GOF *Shp2*$^{E76K/+}$ mice

(A) Scatterplot analysis (SPA) showing that BTK and p110δ inhibition differentially affects gene expression in GOF *Shp2*$^{E76K/+}$ mice in response to drug treatment. RNA from BM HSC/Ps of vehicle- and drug-treated mice was subjected to whole transcriptome analysis. Gene expression changes with p value <0.01 and >1.5 or < −1.5-fold change was considered for scatterplot analysis. Top-right quadrant: genes upregulated in BTK and p110δ inhibitor treatment. Lower-left quadrant: genes downregulated in BTK and p110δ inhibitor treatment. Top-left quadrant: genes upregulated in p110δ inhibitor treatment but downregulated in BTK inhibitor treatment. Lower-right quadrant: genes downregulated in p110δ inhibitor and upregulated BTK inhibitor treatment conditions. (B) IPA analysis showing the effect of combined drug treatment on genes involved in regulating inflammation. (C) Quantitative gene expression changes in response to drug treatment. *p < 0.05. Error bars are shown in mean with standard deviation. (D) Gene set enrichment analysis showing the effect of combined drug treatment compared to vehicle treatment group. (E) Heatmap showing the differentially expressed genes related to cell motility, migration, and extravasation in response to individual and combined drug treatment.

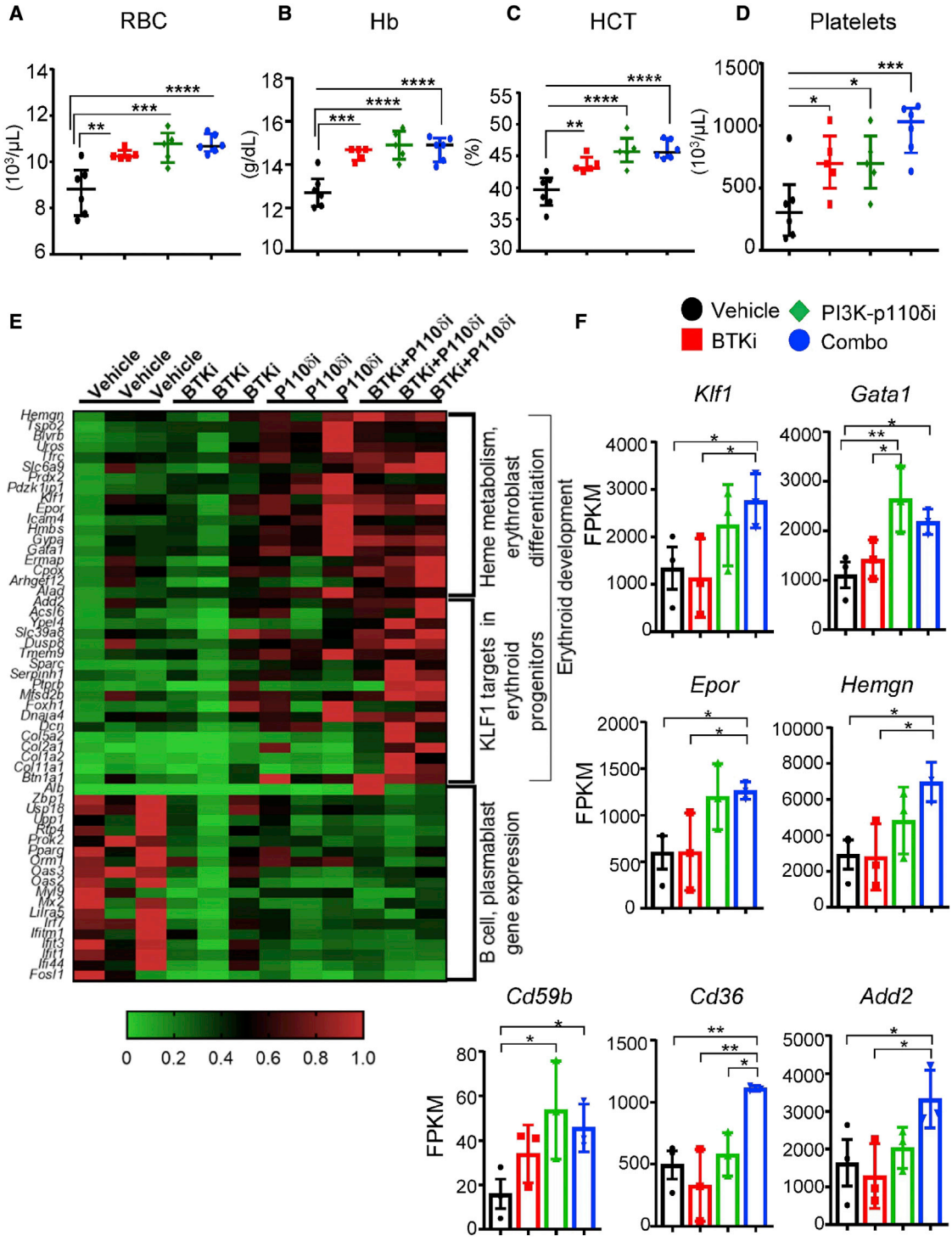

Figure 4. Individual and combined inhibition of BTK and/or PI3K-p110δ rescues erythroid and megakaryocyte deficiencies in GOF Shp2$^{E76K/+}$ mice: PB erythroid parameters in GOF *Shp2*$^{E76K/+}$ mice in response to drug treatment were assessed.

(A) Red blood cells counts. (B) Hemoglobin (Hb). (C) Hematocrits (HCT). (D) PB platelets counts. (E) Heatmap showing the differentially expressed genes related to erythroid growth and differentiation as well as B cell development. (F) Quantitative changes in the expression of genes involved in erythroid/megakaryocyte growth and differentiation. *p < 0.05.Error bars are shown in mean with standard deviation.

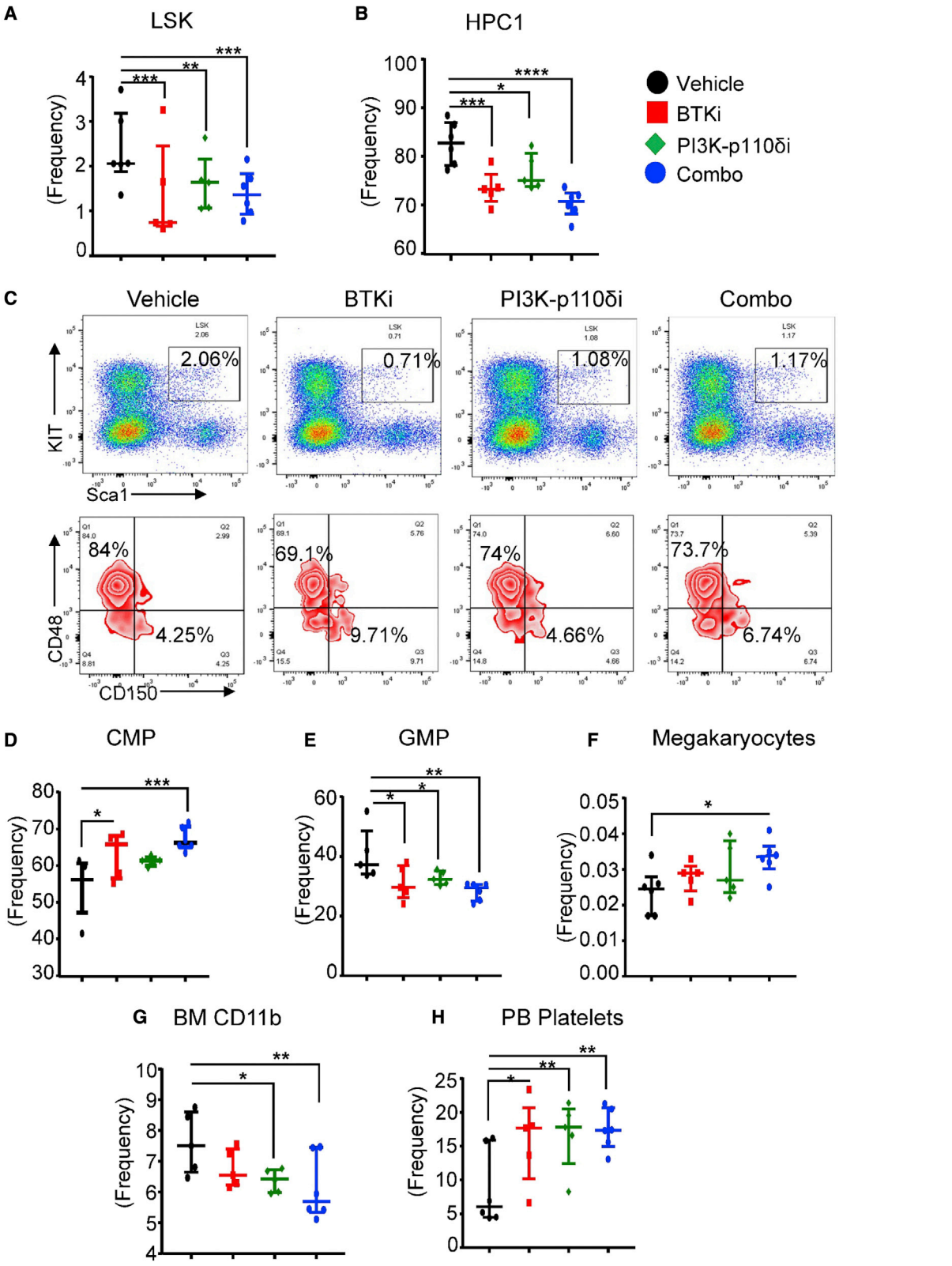

(legend on next page)

PI3K-p110δ induced the differentiation of CMPs to megakaryocytic precursors (Lin^{Neg}, KIT^{Pos}, $CD9^{Pos}$, $CD16/32^{lo}$, $CD41^{Pos}$) more profoundly than into GMPs. As seen in Figure 5F, megakaryocytes are increased uniquely in GOF $Shp2^{E76K/+}$ mice treated with the combination of the two drugs compared to vehicle group or the single-inhibitor-treated group, suggesting that the combined inhibition of BTK and p110δ induces CMPs to differentiate into megakaryocytes. To determine whether the megakaryocyte precursors further differentiate into platelets after drug treatment, we assessed $CD41^{Pos}$ platelets in BM and PB. As seen in Figures 5H, S3A, and S3D, single and combined drug treatment of the BTK and the PI3K-p110δ inhibitor significantly reduced the number of platelets in the BM and increased the platelets in PB compared to the vehicle-treated group. These data suggest that BTK and p110δ inhibition further induces the differentiation of megakaryocytes to platelets and that the differentiated platelets egress into peripheral circulation (Figures 5F, S3C, S3D, and S3E).

Combined inhibition of BTK and PI3K-p110δ in a PDX model of JMML impairs the development of human leukemia stem and progenitor cells

We next investigated whether the combination of these two drugs also impacts the growth and development of patient-derived stem and progenitor cells. We treated PDX mice from a patient with JMML for 34 days, and on the 35th day, we did detailed hematopoietic analysis as outlined in Figure 6A. To delineate the impact of drugs on human leukemic versus murine WT CD45 cells, we gated on human $CD45^{Pos}$ cells to assess the effect of drug treatment on human hematopoiesis, as shown in Figure 6B. While combined drug treatment did not have any effect on normal murine CD45 cells (y axis; Figure 6B), it significantly inhibited the frequency of human $CD45^{Pos}$ cells in the BM (x axis; Figures 6B and 6C(i)). Importantly, the frequency of human $CD45^{Pos}$ lineage negative $CD38^{Neg}CD34^{Pos}$ leukemic stem cells was also significantly decreased by the combined drug treatment compared to vehicle controls (Figures 6B and 6C(ii)). Consistent with the observation noted in the GOF $Shp2^{E76K/+}$ mouse model of human JMML, the frequency of downstream human myeloid progenitors was also significantly impacted. To identify CMP, GMP, and MEP progenitors, we performed gating on human $CD45^{Pos}Lin^{Neg}CD38^{Pos}CD34^{Pos}$ as shown in Figure 6B. As seen in Figure 6C ((iii) to (v)), a greater reduction in the frequency of these progenitors was observed in the drug-treated group compared to controls. These data suggest that the combined drug treatment not only inhibits the expansion of human $CD45^{Pos}$ cells including lin-$CD38^{Neg}$ $CD34^{Pos}$ cells, but it also impacts the development of downstream progenitors.

Gene expression changes in response to drug treatment in JMML patient cells

In an effort to correlate the gene expression changes in GOF $Shp2^{E76K/+}$ mice in response to drug treatment with those observed in human JMML cells, we analyzed the human bulk RNA-seq data from JMML patients and compared the expression of these genes with healthy individuals. Out of 153 genes examined from GOF $Shp2^{E76K/+}$ mice, 50 genes showed statistically significant changes in human RNA-seq data similar to those observed in GOF $Shp2^{E76K/+}$-treated mice. Out of the 50 genes with statistically significant changes in GOF $Shp2^{E76K/+}$ mice upon drug treatment, 42 genes were upregulated (Figure 7A(i)) and eight genes were downregulated (Figure 7B(i)) in JMML patients compared to healthy individuals, as shown in the Venn diagram (Figures 7A and 7B). Out of 42 upregulated genes in JMML patients compared to healthy individuals, 10 genes (*Gsn, Arpc1b Actb, Mapk3, Itgam, Vasp, Itgb2, Usp18, Oas3, Irf7*) (Figure 7C) were found to be downregulated in response to combined drug treatment in GOF $Shp2^{E76K/+}$ mice (Figure 7A(ii)). The majority of these genes (*Gsn*,[38] *Arpc1b*,[39] *Actb*,[40–42] *Mapk3*, *Itgam*,[43] *Vasp*, and *Itgb2*) are involved in cell motility, extravasation, and migration, along with lymphoid cell development (*Usp18*,[44,45] *Oas3*,[46] *Irf7*[47]). All of these genes demonstrated a significant correlation in their expression with the modulation of genes observed in the GOF $Shp2^{E76K/+}$ mice treated with the combination of the two drugs (Figure 7C). Out of eight downregulated genes in JMML patients compared to healthy individuals, 7 genes (*Slc25a38, Cdr2, Ninl, Secl1412, Ntn4, Chst10, Dusp8*) (Figure 7D) were found to be upregulated in response to combined drug treatment in GOF $Shp2^{E76K/+}$ mice (Figure 7B(ii)). Genes involved in hematopoiesis (*Slc25a38*,[48] *Cdr2, Ninl*[49–51]), myelopoiesis (*Secl1412*,[52] *Ntn4*,[53] *Chst10*), and erythropoiesis (*Dusp8*) showed a significant correlation with genes modulated upon drug treatment in the GOF $Shp2^{E76K/+}$ mice (Figure 7D). Overall, a comparative analysis of our RNA-seq data suggests a significant correlation between genes that are significantly up- or downregulated in JMML patients as well as in the HSC/Ps of GOF $Shp2^{E76K/+}$ mice and associated with disease pathology. These genes are significantly modulated in response to combined drug treatment in GOF $Shp2^{E76K/+}$ mice, which is associated with disease correction.

DISCUSSION

We demonstrate that BTK is hyperphosphorylated in GOF $Shp2^{E76K/+}$ myeloid cells and that B cell adaptor for PI3K (BCAP) plays a role in cooperating with PI3K-p110δ. We show that dual inhibition of BTK and PI3K-p110δ results in downregulation of both Erk and Akt *in vitro*. *In vivo*, individual drug treatment with either BTK or PI3K-p110δ inhibitors in primary $Shp2^{E76K/+}$ mice equally rescues erythroid

Figure 5. Impact of single and/or combined drug treatment on stem and progenitor cells bearing GOF $Shp2^{E76K/+}$ mutation

Detailed analysis of BM cells after drug treatment. Quantification of (A) frequency of LSK (Lin^- Kit^+, $Sca1^+$) cells. (B) Frequency of HPC1 (CD48+, CD150-LSK) within LSK gated cells. (C) Upper panel shows representative flow profile of LSK cells, and lower panels show representative flow profiles of HSC/HPC1 cells. (D) Frequency of CMPs (Lin^- $Kit^+CD34^+CD16/32^-$). (E) Frequency of GMPs (Lin^- Kit^+ $CD34^+CD16/32^+$). (F) Frequency of megakaryocytes (Lin^-Kit^+, $CD9^+$ $CD16/32^{lo}$ $CD41^+$). (G) Frequency of BM CD11b+ cells. (H) Frequency of PB platelets. Each data point represents value from individual mice in their respective groups. Error bars in median values of each group are shown with interquartile range. Statistical analysis was performed using GraphPad version 7 by one-way ANOVA with uncorrected Fisher's test. *$p < 0.05$, **$p < 0.01$, ***$p < 0.001$, ****$p < 0.0001$.

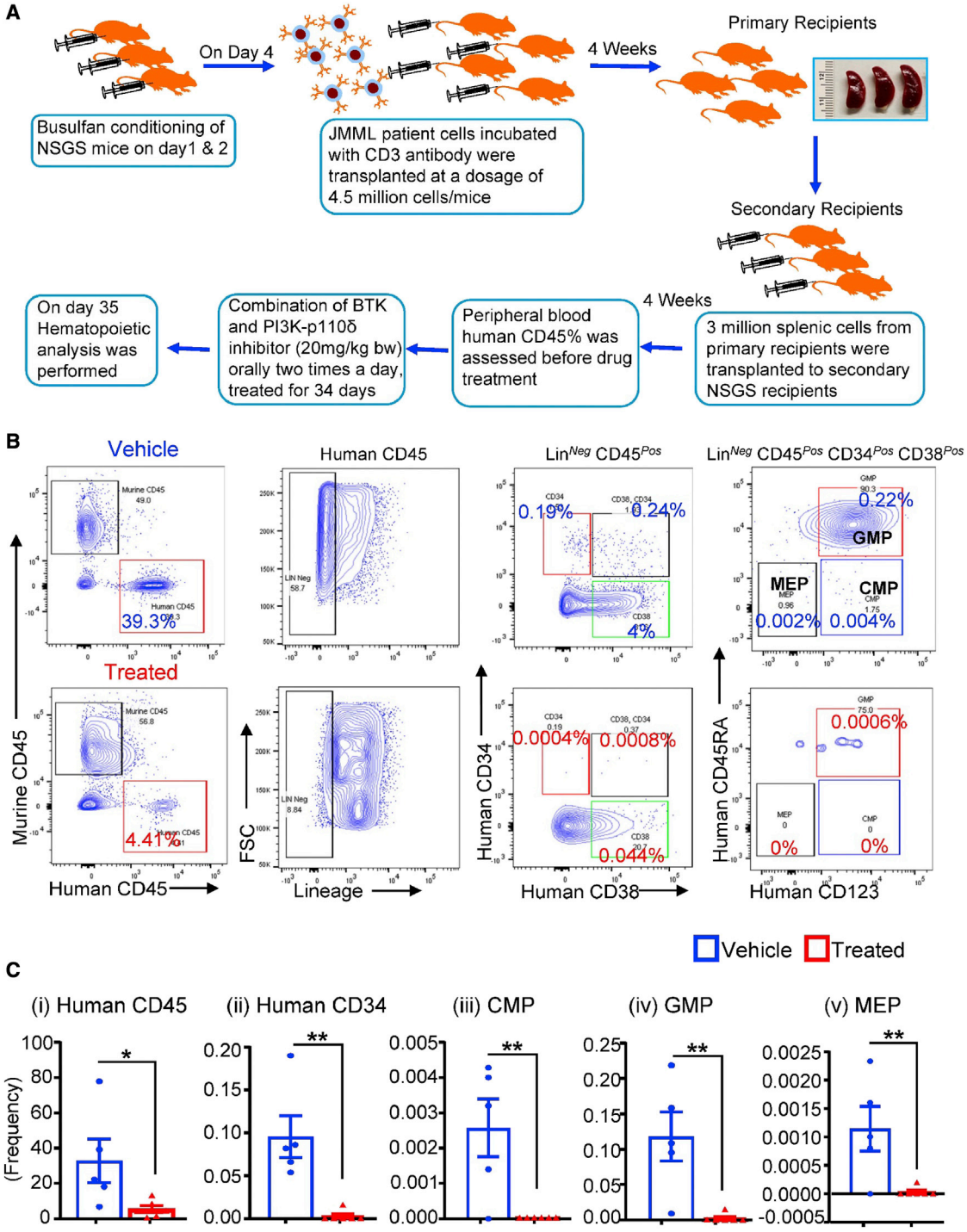

Figure 6. Combined inhibition of BTK and PI3K-p110δ in a PDX model of JMML impairs the development of human leukemia stem and progenitor cells

(A) Schematic of experimental design. (B) Flow prolife showing the effect of combined drug treatment on human JMML hematopoietic stem cells HSC (human $CD45^{Pos}Lin^{Neg}CD38^{Neg}CD34^{Pos}$) and progenitors including CMPs (human $CD45^{Pos}Lin^{Neg}CD38^{Pos}CD34^{Pos}CD123^{Pos}CD45RA^{Neg}$), GMPs (human $CD45^{Pos}Lin^{Neg}CD38^{Pos}CD34^{Pos}CD123^{Pos}CD45RA^{Pos}$), and MEPs (human $CD45^{Pos}Lin^{Neg}CD38^{Pos}CD34^{Pos}CD123^{Neg}CD45RA^{Neg}$). (C) Effect of combined drug treatment on (i) human JMML $CD45^{Pos}$ cells, (ii) human JMML $CD45^{Pos}Lin^{Neg}CD38^{Neg}CD34^{Pos}$ cells, (iii) CMPs, (iv) GMPs, and (v) MEPs. Error bars are shown in median values of each group with interquartile range.

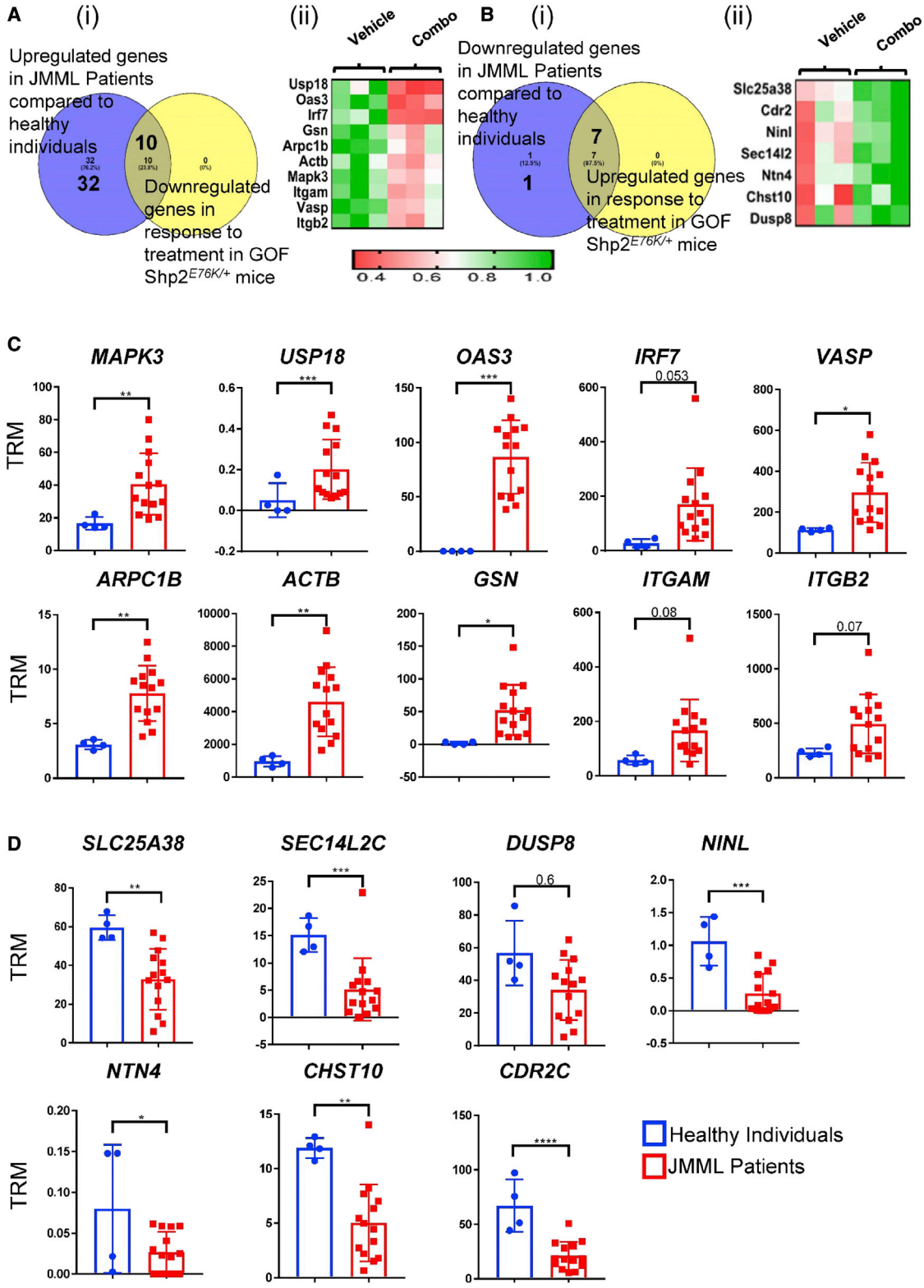

(legend on next page)

parameters, monocytosis, and splenomegaly, whereas combined treatment also profoundly rescues thrombocytopenia.

Our RNA-seq analysis revealed possible molecular mechanism(s) behind the rescue of erythroid and megakaryocyte parameters observed in the current study. Slc25a38 (solute carrier family 25 member 38) a glycine transporter, transports glycine to mitochondrial matrix, thus providing glycine for heme biosynthesis, which is required for erythropoiesis. We found Slc25a38 to be downregulated in JMML patients compared to healthy individuals. It is conceivable that defective heme synthesis and impaired hemoglobin production impairs erythroid cell maturation in JMML patients, thereby leading to anemia. Autosomal recessive pathogenic variants in the mitochondrial glycine transporter SLC25A38 have been implicated in a subset of patients with congenital sideroblastic anemia.[48] The rescue of anemic features including RBC counts, hemoglobin content, and hematocrits observed in drug-treated mice correlates with upregulation of Slc25a38 in response to combined drug treatment in GOF $Shp2^{E76K/+}$ mice, suggesting that combined drug treatment corrects impaired erythropoiesis by at least partly modulating the expression of *Slc25a38* as well as additional genes such as *klf, EpoR, Gata1, Hemgn, CD56*, and *Add2*. Our RNA-seq data demonstrating an increase in the expression of *Gata1* and *cd36* are consistent with the recent single-cell RNA-seq analysis described in JMML.[54]

The substantial rescue in the infiltration of leukemic cells in the spleen, liver, and lung of GOF $Shp2^{E76K/+}$-bearing mice treated with the inhibitors is associated with an impact on genes involved in cell motility, migration, and extravasation. We see Ras homology family V (RhoV) to be downregulated in mice treated with drugs. A similar reduction in the expression of myosin light chain 9 (*Myl9*), an important factor in Rho GTPase signaling and cytoskeleton remodeling by Rho GTPases, was observed in drug-treated mice.

Finally, we also validated the effect of drug treatment observed in primary GOF $Shp2^{E76K/+}$ mice in a human *PTPN11* mutant bearing JMML PDX model system. Louka et al.[54] demonstrated significant heterogeneity in the content of leukemic stem cells in JMML patients. We show a profound impact on these populations in our PDX model using the combination of the two drugs. In summary, given the prevalence of Ras pathway mutations in hematological malignancies, our combined inhibition strategy is advantageous because it allows a lower dose of each drug to be used to attain efficacy with less risk of toxicity. In addition, we are targeting signaling molecules with very restricted expression in the hematopoietic cells to further minimize toxicity. Our findings make for a strong case for the use of BTK inhibitors alone or in combination with p110δ inhibitor for the treatment of human JMML for which no effective targeted therapies currently exist.

MATERIALS AND METHODS

Mice

GOF $Shp2^{E76K/+}$:LysM Cre mice were used for the current study. GOF $Shp2^{E76K/+}$:LysM Cre mice have been described earlier,[55] referred to as GOF $Shp2^{E76K/+}$ mice. All studies were approved by Indiana University Laboratory Animal Resource Center. All animals were maintained in a pathogen-free facility at Indiana University School of Medicine, Indianapolis.

In vivo drug treatment of primary $Shp2^{E76K/+}$ mice

A solution of 0.5% w/v methylcellulose (Sigma Cat #M0262) and 0.1% v/v Tween-80 (Fishers Scientific Cat # BP338) was made in water and treated for vehicle control group. Using vehicle solution, a stock of drug inhibitor (BTK inhibitor, ACP-196 [acalabrutinib], or PI3K p110δ inhibitor, ACP-319; provided to us by Acerta Pharma) was made, aliquoted into 1-mL aliquots, and stored at 4°C during the 21 days of treatment. Prior to each dosing, the necessary amount of drug and vehicle were brought to room temperature and mixed thoroughly. Mice were dosed BID (twice a day) via oral gavage.

Generation of patient-derived xenografts and *in vivo* drug treatment

The triple transgenic NSG-SGM3 (NSGS) mice expressing human IL3, GM-CSF (CSF2), and SCF (KITLG) mice were obtained from Indiana University *In vivo* Therapeutics Core facility. The number of both male and female mice were distributed equally in both vehicle-treated and combination-drug-treated groups used in this experiment. All the NSGS mice were between 11 and 14 weeks of age. NSGS mice conditioning and xenotransplantation was performed as described.[56–58] Briefly, NSGS mice were conditioned with intraperitoneal injection of busulfan at 12.5 mg/kg bw for 2 consecutive days, and after 48 h, *PTPN11* mutated patient-derived cells were injected via tail vein. *PTPN11* donor cells were incubated with anti-CD3 (OTK3) antibody for 30 min on ice, and 4.5 million cells per mouse were injected as primary transplants. Four weeks after primary transplantation, three million cells from primary transplanted mice spleens were harvested and transplanted into secondary NSGS mice after busulfan conditioning. Drug studies were conducted in secondary transplants. Human CD45-positive cells were assessed in PB after 3 to 4 weeks of secondary transplantation. Based on the percentage of CD45-positive cells, the experimental mice were separated into vehicle- and dual-drug-treated groups similar to primary mice treatment regimen of 20 mg/kg body weight of BTK and PI3K-p110δ

Figure 7. Gene expression changes in response to drug treatment in JMML patient cells

(A) (i) Venn diagram showing genes upregulated in JMML patients that were downregulated in response to drug treatment in GOF $Shp2^{E76K/+}$ mice. (ii) Heatmap showing the list of genes downregulated in GOF $Shp2^{E76K/+}$ mice in response to drug treatment, while upregulated in JMML patients compared to healthy individuals. (B) (i) Venn diagram showing the genes downregulated in JMML patients, which were upregulated in response to drug treatment in GOF $Shp2^{E76K/+}$ mice. (ii) Heatmap showing the list of genes upregulated in GOF $Shp2^{E76K/+}$ mice in response to drug treatment, while downregulated in JMML patients compared to healthy individuals. (C) Genes upregulated in JMML patients compared to healthy individuals. *$p < 0.05$. (D) Genes downregulated in JMML patients compared to healthy individuals. *$p < 0.05$, **$p < 0.01$, *** $p < 0.001$, **** $p < 0.0001$. Error bars are shown in mean with standard deviation.

inhibitor for 34 days. On day 35 the impact of drug treatment was studied in the BM, spleen, and PB.

RNA sequencing, differential gene expression, and pathway enrichment analysis

RNA was extracted from single-cell suspension of BM cells in RLT (lysis buffer for lysing cells and tissues prior to RNA isolation) buffer using the RNeasy Plus Micro Kit (Qiagen, Cat # 74,034) per manufacturer's instructions. RNA was sequenced at the Center for Medical Genomics, Indiana University School of Medicine, as described. We analyzed RNA-seq data as described in our earlier studies.[13] Briefly, RNA integrity and concentration were assessed using Agilent 2100 Bioanalyzer to assess the quantity and size distribution of the library preparation. A Phred quality score was used to confirm the sequencing quality. The sequencing data was next assessed using FastQC (Babraham bioinformatics, Cambridge, UK) and then mapped to mouse genome (UCSC mm10) using STAR RNA-seq aligner with the parameter "outSAMmapqUNIQUE 60."[59] Raw primary mice RNA-seq data has been approved by NCBI GEO database with accession code GSE: 185552. Human bulk RNA-seq data from JMML patients was obtained from a previous publication.[60] The raw data can be found in dbGaP with the accession reference of phs000973.V1.p.

Adherent macrophage cell culture

Primary murine low-density mononuclear cells were cultured in IMDM, 20% FBS, 2% penicillin/streptomycin, and 25 ng/mL macrophage colony stimulating factor (M-CSF) for 7–10 days at 37°C and 5% CO_2 to generate adherent macrophage progenitors. The media was changed after cells became adherent at day 5 and every 2 days thereafter.

Isolation of total cellular protein lysates

Cells were washed twice in cold PBS and incubated on ice for 5–10 min in a lysis buffer containing 50 mM HEPES, 150 mM NaCl, 10% glycerol, 1% Triton X-, 1.5 mM $MgCl_2$, 1 mM EGTA, 100 mM NaF, and 10 mM NaPPi with Na_3VO_4, $ZnCl_2$, PMSF, and protease inhibitor cocktail (Sigma #P8340). Protein lysates were collected by scraping, then centrifuged at 13,200 rpm for 15 min at 4°C and quantified using Bradford reagent.

Immunoblot analysis

Protein lysates were separated by SDS-polyacrylamide gel electrophoresis and transferred to nitrocellulose membrane, which was then incubated with shaking overnight in primary antibody at 4°C. The membrane was then washed and incubated with HRP-conjugated secondary antibody and developed with Super Signal (Thermo Scientific, #1859024 and #1859025) and exposed by using a Bio-Rad Imager.

Immunoprecipitation

Equal amounts of fresh protein lysates per sample were aliquoted into 1.5-mL Eppendorf tubes, volumes were equalized with lysis buffer, HNTG buffer (1% Triton X-, 50 mM HEPES, 50 mM NaCl, 5 mM EDTA, 0.1% BSA, 50 mM NaF with Na_3VO_4, $ZnCl_2$, PMSF, and protease inhibitor cocktail) was added to bring total volume to 500 μL, and anti-BCAP antibody was added. Tubes were rotated at 4°C for 2 h, then 25 μL of HNTG-washed Protein A/G PLUS-Agarose beads (Santa Cruz) were added per tube. Tubes were rotated at 4°C overnight, then washed three times with wash buffer (1% Triton X-, 50 mM HEPES, 120 mM NaCl, 5 mM EDTA, 50 mM NaF with Na_3VO_4, $ZnCl_2$, PMSF, and protease inhibitor cocktail) for 15 min at 4°C rotating, spinning down at 3,000 rpm for 30 s in between washes, and used for immunoblotting analysis.

Preparation of single-cell suspension and flow cytometry analysis

For the analysis of primary transplanted mice, PB counts were assessed using Element HT5 hematology analyzer (Heska, USA). Experimental mice were euthanized after 3 weeks of treatment, and a single-cell suspension of BM, spleen, and PB was prepared. BM was flushed using IMDM, and spleen was crushed between the microscopic slides followed by RBC lysis to prepare single-cell suspension. An aliquot of single-cell BM suspension was resuspended in RLT buffer (Qiagen, Cat# 79216) for RNA-seq analysis and saved in −80°C until used. Another aliquot of single-cell suspension was blocked in 10% rat serum in PBS for flow cytometry analysis. Flow cytometry analysis was performed as previously described.[61] Cells were acquired using BD Canto II flow machine, and the data was analyzed using FlowJo Software. All flow cytometry antibodies were purchased from Biolegend, unless otherwise specified. Briefly, cells were stained with PE conjugated lineage antibodies, Ter119 PE (Cat# 116208), B220 PE (Cat# 103208), Gr1 PE (Cat# 108408), CD11b PE (Cat# 101208), and CD3 PE (Cat# 100308), to separate lineage-negative and lineage-positive population. Gating on lineage-negative Kit^{Pos} (APC, Cat# 105812), $Sca1^{Pos}$ (PE Cy7, Cat# 122514), $CD48^{Neg}$ (APC Cy7, Cat# 103432), and $CD150^{Pos}$ (PerCP Cy5.5, Cat# 115922) subsets of LSK population including HSC (hematopoietic stem cells, long-term HSC), HPC1, and hematopoietic progenitor-2 populations were determined. Lineage-negative KIT^{Pos} cells were gated to detect committed progenitors including CMP (Lin^{Neg}, KIT^{Pos}, $CD16/32^{Neg}$, $CD34^{Pos}$), GMP (Lin^{Neg}, KIT^{Pos}, $CD16/32^{Pos}$, $CD34^{Pos}$), MEP (Lin^{Neg}, KIT^{Pos}, $CD16/32^{Neg}$, $CD34^{Neg}$), and megakaryocytic progenitors (Lin^{Neg}, KIT^{Pos}, $CD9^{Pos}$, $CD16/32^{lo}$, $CD41^{Pos}$).

To detect committed progenitors, the following antibodies were used: Lineage PE, Ter119 PE (Cat# 116208), B220 PE (Cat# 103208), Gr1 PE (Cat# 108408), CD11b PE (Cat# 101208), CD3 PE (Cat# 100308), Sca1 PerCP Cy5.5 (Cat# 122524), KIT-APC Cy7 (Cat# 105826), CD16/32 PE Cy7 (Cat# 101318), CD34 FITC (BD Biosciences, Cat# 553733), CD19 APC (Biosciences, Cat# 17-0193-80), CD9 FITC (Cat# 124808), and CD41-APC (Cat# 133914). Mature differentiated cells were detected by staining with Gr1-APC Cy7 (Cat# 108424), CD11b -PE (Cat# 101208), B220 – APC (Cat# 103212), and CD3-PE Cy7 (Cat# 100220).

All human flow antibodies were procured from Biolegend. Single-cell suspension from xenograft experimental mice BM was prepared

similar to primary mice as mentioned above. PB and BM single-cell suspensions were blocked with True stain Human Fc receptor blocking solution (Cat# 422302) and stained with different antibodies. Gating strategy for detecting subsets of human hematopoietic stem and committed progenitor cells was assessed as described.[62] Briefly, murine and human cells were separated by staining with anti-mouse CD45 APC (Cat# 103112) and anti-human CD45 PE (Cat# 304008) antibodies. By gating on human $CD45^{Pos}$ population, lineage-negative cells were detected by staining with FITC lineage (Cat# 348801) antibody cocktail, which was further sub-fractionated into $CD34^{Pos}$ (APC Cy7, Cat# 343514) and $CD38^{Neg}$ (PE Cy5, Cat# 303508) stem cells. Further gating on CD34/CD38 double-positive population, committed progenitors, including CMPs (human $CD45^{Pos}$, Lin^{Neg}, $CD123^{Pos}$, $CD45RA^{Neg}$), GMPs (human $CD45^{Pos}$, Lin^{Neg}, $CD123^{Pos}$, $CD45RA^{Pos}$), and MEPs (Human $CD45^{Pos}$, Lin^{Neg}, $CD123^{Neg}$, $CD45RA^{Neg}$) was detected by staining with CD123 PE Cy7 (Cat# 306010) and CD45RA BV421 (Cat# 304130) antibodies.

Histopathological analysis

Spleen, liver, and lungs from vehicle- and drug-treated groups of mice were fixed in formalin, sectioned, and stained with hematoxylin and eosin (H&E). All images were acquired at 20x magnification with a 200-μm scale bar.

Statistical analysis

One-way ANOVA analysis was performed for comparing between more than two groups to determine significant differences using Prism software. Student's t test was performed to compare between two groups.

SUPPLEMENTAL INFORMATION

Supplemental information can be found online at https://doi.org/10.1016/j.ymthe.2022.04.009.

ACKNOWLEDGMENTS

We would like to thank Dr. Ping Hu and Ms. Tracy Winkle for their administrative support. This work was supported by NIH grants R01CA173852, R01CA134777, R01HL146137, and R01HL140961, and Riley Children's Foundation (to R.K.). We thank Acerta Pharmaceuticals for proving us with the BTK and p110δ inhibitors.

AUTHOR CONTRIBUTIONS

B.R., L.Y., R.C., L.H., and R.K. conceptualized the study, designed the experiment, analyzed the data, and wrote the manuscript. L.R.P. performed RNA-seq analysis and wrote the manuscript. Z.C. performed RNA-seq analysis. R.P. assisted with *in vivo* studies and analyzed the data. S.K.P., R.P., J.Z., V.J., and R.K. assisted with experiments. C.M. and G.S. performed histopathology analysis. E.W., C.Z., and E.S. provided JMML patient samples and human JMML RNA-seq data. All authors read the manuscript.

DECLARATION OF INTEREST

The authors declare no competing interests.

REFERENCES

1. Loh, M.L. (2011). Recent advances in the pathogenesis and treatment of juvenile myelomonocytic leukaemia. Br. J. Haematol. *152*, 677–687. https://doi.org/10.1111/j.1365-2141.2010.08525.x.

2. Emanuel, P.D., Bates, L.J., Castleberry, R.P., Gualtieri, R.J., and Zuckerman, K.S. (1991). Selective hypersensitivity to granulocyte-macrophage colony-stimulating factor by juvenile chronic myeloid leukemia hematopoietic progenitors. Blood *77*, 925–929. https://doi.org/10.1182/blood.v77.5.925.bloodjournal775925.

3. Bergstraesser, E., Hasle, H., Rogge, T., Fischer, A., Zimmermann, M., Noellke, P., and Niemeyer, C.M. (2007). Non-hematopoietic stem cell transplantation treatment of juvenile myelomonocytic leukemia: a retrospective analysis and definition of response criteria. Pediatr. Blood Cancer *49*, 629–633. https://doi.org/10.1002/pbc.21038.

4. Locatelli, F., Nollke, P., Zecca, M., Korthof, E., Lanino, E., Peters, C., Pession, A., Kabisch, H., Uderzo, C., Bonfim, C.S., et al. (2005). Hematopoietic stem cell transplantation (HSCT) in children with juvenile myelomonocytic leukemia (JMML): results of the EWOG-MDS/EBMT trial. Blood *105*, 410–419. https://doi.org/10.1182/blood-2004-05-1944.

5. Chang, Y.H., Jou, S.T., Lin, D.T., Lu, M.Y., and Lin, K.H. (2004). Second allogeneic hematopoietic stem cell transplantation for juvenile myelomonocytic leukemia: case report and literature review. J. Pediatr. Hematol. Oncol. *26*, 190–193. https://doi.org/10.1097/00043426-200403000-00009.

6. Inagaki, J., Fukano, R., Nishikawa, T., Nakashima, K., Sawa, D., Ito, N., and Okamura, J. (2013). Outcomes of immunological interventions for mixed chimerism following allogeneic stem cell transplantation in children with juvenile myelomonocytic leukemia. Pediatr. Blood Cancer *60*, 116–120. https://doi.org/10.1002/pbc.24259.

7. Yoshimi, A., Mohamed, M., Bierings, M., Urban, C., Korthof, E., Zecca, M., Sykora, K.W., Duffner, U., Trebo, M., Matthes-Martin, S., et al.; On behalf of the European Working Group of MDS in Childhood EWOG-MDS (2007). Second allogeneic hematopoietic stem cell transplantation (HSCT) results in outcome similar to that of first HSCT for patients with juvenile myelomonocytic leukemia. Leukemia *21*, 556–560. https://doi.org/10.1038/sj.leu.2404537.

8. Chang, T.Y., Dvorak, C.C., and Loh, M.L. (2014). Bedside to bench in juvenile myelomonocytic leukemia: insights into leukemogenesis from a rare pediatric leukemia. Blood *124*, 2487–2497. https://doi.org/10.1182/blood-2014-03-300319.

9. de Vries, A.C., Zwaan, C.M., and van den Heuvel-Eibrink, M.M. (2010). Molecular basis of juvenile myelomonocytic leukemia. Haematologica *95*, 179–182. https://doi.org/10.3324/haematol.2009.016865.

10. Kratz, C.P., Niemeyer, C.M., Castleberry, R.P., Cetin, M., Bergstrasser, E., Emanuel, P.D., Hasle, H., Kardos, G., Klein, C., Kojima, S., et al. (2005). The mutational spectrum of PTPN11 in juvenile myelomonocytic leukemia and Noonan syndrome/myeloproliferative disease. Blood *106*, 2183–2185. https://doi.org/10.1182/blood-2005-02-0531.

11. Tartaglia, M., Niemeyer, C.M., Fragale, A., Song, X., Buechner, J., Jung, A., Hahlen, K., Hasle, H., Licht, J.D., and Gelb, B.D. (2003). Somatic mutations in PTPN11 in juvenile myelomonocytic leukemia, myelodysplastic syndromes and acute myeloid leukemia. Nat. Genet. *34*, 148–150. https://doi.org/10.1038/ng1156.

12. Chen, Y.N.P., LaMarche, M.J., Chan, H.M., Fekkes, P., Garcia-Fortanet, J., Acker, M.G., Antonakos, B., Chen, C.H.T., Chen, Z., Cooke, V.G., et al. (2016). Allosteric inhibition of SHP2 phosphatase inhibits cancers driven by receptor tyrosine kinases. Nature *535*, 148–152. https://doi.org/10.1038/nature18621.

13. Pandey, R., Ramdas, B., Wan, C., Sandusky, G., Mohseni, M., Zhang, C., and Kapur, R. (2019). SHP2 inhibition reduces leukemogenesis in models of combined genetic and epigenetic mutations. J. Clin. Invest. *129*, 5468–5473. https://doi.org/10.1172/JCI130520.

14. Goodwin, C.B., Li, X.J., Mali, R.S., Chan, G., Kang, M., Liu, Z., Vanhaesebroeck, B., Neel, B.G., Loh, M.L., Lannutti, B.J., et al. (2014). PI3K p110δ uniquely promotes gain-of-function Shp2-induced GM-CSF hypersensitivity in a model of JMML. Blood *123*, 2838–2842. https://doi.org/10.1182/blood-2013-10-535104.

15. Lucas, F., and Woyach, J.A. (2019). Inhibiting Bruton's tyrosine kinase in CLL and other B-cell malignancies. Target Oncol. *14*, 125–138. https://doi.org/10.1007/s11523-019-00635-7.

16. Fan, Z., Li, Y., Xia, L., and Wu, Y. (2021). Knockout of Bruton's tyrosine kinase in macrophages attenuates diabetic nephropathy in streptozotocin-induced mice. Am. J. Transl. Res. *13*, 12352–12363.

17. Qiu, J., Fu, Y., Chen, Z., Zhang, L., Li, L., Liang, D., Wei, F., Wen, Z., Wang, Y., and Liang, S. (2021). BTK promotes atherosclerosis by regulating oxidative stress, mitochondrial injury, and ER stress of macrophages. Oxid. Med. Cell Longev. *2021*, 9972413. https://doi.org/10.1155/2021/9972413.

18. Rushworth, S.A., Murray, M.Y., Zaitseva, L., Bowles, K.M., and MacEwan, D.J. (2014). Identification of Bruton's tyrosine kinase as a therapeutic target in acute myeloid leukemia. Blood *123*, 1229–1238. https://doi.org/10.1182/blood-2013-06-511154.

19. Watanabe, D., Hashimoto, S., Ishiai, M., Matsushita, M., Baba, Y., Kishimoto, T., Kurosaki, T., and Tsukada, S. (2001). Four tyrosine residues in phospholipase C-gamma 2, identified as Btk-dependent phosphorylation sites, are required for B cell antigen receptor-coupled calcium signaling. J. Biol. Chem. *276*, 38595–38601. https://doi.org/10.1074/jbc.M103675200.

20. Kim, Y.J., Sekiya, F., Poulin, B., Bae, Y.S., and Rhee, S.G. (2004). Mechanism of B-cell receptor-induced phosphorylation and activation of phospholipase C-γ2. Mol. Cell Biol. *24*, 9986–9999. https://doi.org/10.1128/MCB.24.22.9986-9999.2004.

21. Rodriguez, R., Matsuda, M., Perisic, O., Bravo, J., Paul, A., Jones, N.P., Light, Y., Swann, K., Williams, R.L., and Katan, M. (2001). Tyrosine residues in phospholipase Cγ2 essential for the enzyme function in B-cell signaling. J. Biol. Chem. *276*, 47982–47992. https://doi.org/10.1074/jbc.M107577200.

22. Okada, T., Maeda, A., Iwamatsu, A., Gotoh, K., and Kurosaki, T. (2000). BCAP: the tyrosine kinase substrate that connects B cell receptor to phosphoinositide 3-kinase activation. Immunity *13*, 817–827. https://doi.org/10.1016/s1074-7613(00)00079-0.

23. Ni, M.J., MacFarlane, A.W., Toft, M., Lowell, C.A., Campbell, K.S., and Hamerman, J.A. (2012). B-cell adaptor for PI3K (BCAP) negatively regulates Toll-like receptor signaling through activation of PI3K. Proc. Natl. Acad. Sci. U S A *109*, 267–272. https://doi.org/10.1073/pnas.1111957108.

24. Xia, H., Qi, H., Li, Y., Pei, J., Barton, J., Blackstad, M., Xu, T., and Tao, W. (2002). LATS1 tumor suppressor regulates G2/M transition and apoptosis. Oncogene *21*, 1233–1241. https://doi.org/10.1038/sj.onc.1205174.

25. Wu, Y., Wang, S., Farooq, S.M., Castelvetere, M.P., Hou, Y., Gao, J.L., Navarro, J.V., Oupicky, D., Sun, F., and Li, C. (2012). A chemokine receptor CXCR2 macromolecular complex regulates neutrophil functions in inflammatory diseases. J. Biol. Chem. *287*, 5744–5755. https://doi.org/10.1074/jbc.M111.315762.

26. Boyle, K., Egan, P., Rakar, S., Willson, T.A., Wicks, I.P., Metcalf, D., Hilton, D.J., Nicola, N.A., Alexander, W.S., Roberts, A.W., and Robb, L. (2007). The SOCS box of suppressor of cytokine signaling-3 contributes to the control of G-CSF responsiveness in vivo. Blood *110*, 1466–1474. https://doi.org/10.1182/blood-2007-03-079178.

27. Wang, P., Wang, Z., and Liu, J. (2020). Role of HDACs in normal and malignant hematopoiesis. Mol. Cancer *19*, 5. https://doi.org/10.1186/s12943-019-1127-7.

28. Taddei, A., Giampietro, C., Conti, A., Orsenigo, F., Breviario, F., Pirazzoli, V., Potente, M., Daly, C., Dimmeler, S., and Dejana, E. (2008). Endothelial adherens junctions control tight junctions by VE-cadherin-mediated upregulation of claudin-5. Nat. Cell Biol. *10*, 923–934. https://doi.org/10.1038/ncb1752.

29. Makkonen, H., Jaaskelainen, T., Pitkanen-Arsiola, T., Rytinki, M., Waltering, K.K., Matto, M., Visakorpi, T., and Palvimo, J.J. (2008). Identification of ETS-like transcription factor 4 as a novel androgen receptor target in prostate cancer cells. Oncogene *27*, 4865–4876. https://doi.org/10.1038/onc.2008.125.

30. Wright, J.H., Munar, E., Jameson, D.R., Andreassen, P.R., Margolis, R.L., Seger, R., and Krebs, E.G. (1999). Mitogen-activated protein kinase kinase activity is required for the G(2)/M transition of the cell cycle in mammalian fibroblasts. Proc. Natl. Acad. Sci. U S A *96*, 11335–11340. https://doi.org/10.1073/pnas.96.20.11335.

31. Huang, C., Du, R., Jia, X., Liu, K., Qiao, Y., Wu, Q., Yao, N., Yang, L., Zhou, L., Liu, X., et al. (2022). CDK15 promotes colorectal cancer progression via phosphorylating PAK4 and regulating beta-catenin/MEK-ERK signaling pathway. Cell Death Differ. *29*, 14–27. https://doi.org/10.1038/s41418-021-00828-6.

32. Chen, Y.Y., Liu, Y.F., Liu, Y.D., Deng, X.H., and Zhou, J. (2021). IRF7 suppresses hematopoietic regeneration under stress via CXCR4. Stem Cells *39*, 183–195. https://doi.org/10.1002/stem.3308.

33. Lin, Y., Li, X.Y., Willis, A.L., Liu, C., Chen, G., and Weiss, S.J. (2014). Snail1-dependent control of embryonic stem cell pluripotency and lineage commitment. Nat. Commun. *5*, 3070. https://doi.org/10.1038/ncomms4070.

34. Hodge, R.G., and Ridley, A.J. (2020). Regulation and functions of RhoU and RhoV. Small GTPases *11*, 8–15. https://doi.org/10.1080/21541248.2017.1362495.

35. Ambrus, J.L., Jr., Peters, M.G., Fauci, A.S., and Brown, E.J. (1990). The Ba fragment of complement factor B inhibits human B lymphocyte proliferation. J. Immunol. *144*, 1549–1553.

36. Vogler, M. (2012). BCL2A1: the underdog in the BCL2 family. Cell Death Differ. *19*, 67–74. https://doi.org/10.1038/cdd.2011.158.

37. Akiyama, H., Lyons, J.P., Mori-Akiyama, Y., Yang, X., Zhang, R., Zhang, Z., Deng, J.M., Taketo, M.M., Nakamura, T., Behringer, R.R., et al. (2004). Interactions between Sox9 and beta-catenin control chondrocyte differentiation. Genes Dev. *18*, 1072–1087. https://doi.org/10.1101/gad.1171104.

38. Yin, H.L., and Janmey, P.A. (2003). Phosphoinositide regulation of the actin cytoskeleton. Annu. Rev. Physiol. *65*, 761–789. https://doi.org/10.1146/annurev.physiol.65.092101.142517.

39. Kuijpers, T.W., Tool, A.T.J., van der Bijl, I., de Boer, M., van Houdt, M., de Cuyper, I.M., Roos, D., van Alphen, F., van Leeuwen, K., Cambridge, E.L., et al. (2017). Combined immunodeficiency with severe inflammation and allergy caused by ARPC1B deficiency. J. Allergy Clin. Immunol. *140*, 273–277.e10. https://doi.org/10.1016/j.jaci.2016.09.061.

40. Drazic, A., Aksnes, H., Marie, M., Boczkowska, M., Varland, S., Timmerman, E., Foyn, H., Glomnes, N., Rebowski, G., Impens, F., et al. (2018). NAA80 is actin's N-terminal acetyltransferase and regulates cytoskeleton assembly and cell motility. Proc. Natl. Acad. Sci. U S A *115*, 4399–4404. https://doi.org/10.1073/pnas.1718336115.

41. Sorrentino, S., Studt, J.D., Medalia, O., and Tanuj Sapra, K. (2015). Roll, adhere, spread and contract: structural mechanics of platelet function. Eur. J. Cell Biol. *94*, 129–138. https://doi.org/10.1016/j.ejcb.2015.01.001.

42. Sorrentino, S., Conesa, J.J., Cuervo, A., Melero, R., Martins, B., Fernandez-Gimenez, E., De Isidro-Gomez, F.P., de la Morena, J., Studt, J.D., Sorzano, C.O.S., et al. (2021). Structural analysis of receptors and actin polarity in platelet protrusions. Proc. Natl. Acad. Sci. U S A *118*. e2105004118. https://doi.org/10.1073/pnas.2105004118.

43. Bai, M., Grieshaber-Bouyer, R., Wang, J.X., Schmider, A.B., Wilson, Z.S., Zeng, L.L., Halyabar, O., Godin, M.D., Nguyen, H.N., Levescot, A., et al. (2017). CD177 modulates human neutrophil migration through activation-mediated integrin and chemoreceptor regulation. Blood *130*, 2092–2100. https://doi.org/10.1182/blood-2017-03-768507.

44. Arimoto, K.i., Lochte, S., Stoner, S.A., Burkart, C., Zhang, Y., Miyauchi, S., Wilmes, S., Fan, J.B., Heinisch, J.J., Li, Z., et al. (2017). STAT2 is an essential adaptor in USP18-mediated suppression of type I interferon signaling. Nat. Struct. Mol. Biol. *24*, 279–289. https://doi.org/10.1038/nsmb.3378.

45. Yang, L., Jing, Y.K., Kang, D.Q., Jiang, P.P., Li, N., Zhou, X.R., Chen, Y., Westerberg, L.S., and Liu, C.H. (2021). Ubiquitin-specific peptidase 18 regulates the differentiation and function of Treg cells. Genes Dis. *8*, 344–352. https://doi.org/10.1016/j.gendis.2020.03.004.

46. Lee, W.B., Choi, W.Y., Lee, D.H., Shim, H., Kim-Ha, J., and Kim, Y.J. (2019). OAS1 and OAS3 negatively regulate the expression of chemokines and interferon-responsive genes in human macrophages. BMB Rep. *52*, 133–138. https://doi.org/10.5483/BMBRep.2019.52.2.129.

47. Lu, R.Q., and Pitha, P.M. (2001). Monocyte differentiation to macrophage requires interferon regulatory factor 7. J. Biol. Chem. *276*, 45491–45496. https://doi.org/10.1074/jbc.C100421200.

48. Uminski, K., Houston, D.S., Hartley, J.N., Liu, J., Cuvelier, G.D.E., and Israels, S.J. (2020). Clinical characterization and hematopoietic stem cell transplant outcomes for congenital sideroblastic anemia caused by a novel pathogenic variant inSLC25A38. Pediatr. Blood Cancer *67*, e28623. https://doi.org/10.1002/pbc.28623.

49. Casenghi, M., Meraldi, P., Weinhart, U., Duncan, P.I., Korner, R., and Nigg, E.A. (2003). Polo-like kinase 1 regulates Nlp, a centrosome protein involved in microtubule nucleation. Dev. Cell *5*, 113–125. https://doi.org/10.1016/S1534-5807(03)00193-X.

50. Zhao, X.L., Jin, S.Q., Song, Y.M., and Zhan, Q.M. (2010). Cdc2/cyclin B1 regulates centrosomal Nlp proteolysis and subcellular localization. Cancer Biol. Ther. *10*, 945–952. https://doi.org/10.4161/cbt.10.9.13368.

51. Zhang, Y., Morgan, M.J., Chen, K., Choksi, S., and Liu, Z.G. (2012). Induction of autophagy is essential for monocyte-macrophage differentiation. Blood *119*, 2895–2905. https://doi.org/10.1182/blood-2011-08-372383.

52. Li, Z.H., Lou, Y., Tian, G.Y., Wu, J.Y., Lu, A.Q., Chen, J., Xu, B.B., Shi, J.P., and Yang, J. (2019). Discovering master regulators in hepatocellular carcinoma: one novel MR, SEC14L2 inhibits cancer cells. Aging (Albany NY) *11*, 12375–12411. https://doi.org/10.18632/aging.102579.

53. Nacht, M., St Martin, T.B., Martin, T.B.S., Byrne, A., Klinger, K.W., Teicher, B.A., Madden, S.L., and Jiang, Y.D. (2009). Netrin-4 regulates angiogenic responses and tumor cell growth. Exp. Cell Res. *315*, 784–794. https://doi.org/10.1016/j.yexcr.2008.11.018.

54. Louka, E., Povinelli, B., Rodriguez-Meira, A., Buck, G., Elliott, N., Iskander, D., de la Fuente, J., Fordham, N., O'Byrne, S., Inglott, S., et al. (2021). Heterogeneous disease-propagating stem cells in juvenile myelomonocytic leukemia. J. Exp. Med. *218*. e20180853. https://doi.org/10.1084/jem.20180853.

55. Xu, D., Liu, X., Yu, W.M., Meyerson, H.J., Guo, C., Gerson, S.L., and Qu, C.K. (2011). Non-lineage/stage-restricted effects of a gain-of-function mutation in tyrosine phosphatase Ptpn11 (Shp2) on malignant transformation of hematopoietic cells. J. Exp. Med. *208*, 1977–1988. https://doi.org/10.1084/jem.20110450.

56. Chevaleyre, J., Duchez, P., Rodriguez, L., Vlaski, M., Villacreces, A., Conrad-Lapostolle, V., Praloran, V., Ivanovic, Z., and de la Grange, P.B. (2013). Busulfan administration flexibility increases the applicability of scid repopulating cell assay in NSG mouse model. PLoS One *8*, e74361. https://doi.org/10.1371/journal.pone.0074361.

57. Wunderlich, M., Brooks, R.A., Panchal, R., Rhyasen, G.W., Danet-Desnoyers, G., and Mulloy, J.C. (2014). OKT3 prevents xenogeneic GVHD and allows reliable xenograft initiation from unfractionated human hematopoietic tissues. Blood *123*, E134–E144. https://doi.org/10.1182/blood-2014-02-556340.

58. Yoshimi, A., Balasis, M.E., Vedder, A., Feldman, K., Ma, Y., Zhang, H.L., Lee, S.C.W., Letson, C., Niyongere, S., Lu, S.X., et al. (2017). Robust patient-derived xenografts of MDS/MPN overlap syndromes capture the unique characteristics of CMML and JMML (vol 130, pg 397, 2017). Blood *130*, 1602. https://doi.org/10.1182/blood-2017-08-801431.

59. Dobin, A., Davis, C.A., Schlesinger, F., Drenkow, J., Zaleski, C., Jha, S., Batut, P., Chaisson, M., and Gingeras, T.R. (2013). STAR: ultrafast universal RNA-seq aligner. Bioinformatics *29*, 15–21. https://doi.org/10.1093/bioinformatics/bts635.

60. Stieglitz, E., Taylor-Weiner, A.N., Chang, T.Y., Gelston, L.C., Wang, Y.D., Mazor, T., Esquivel, E., Yu, A., Seepo, S., Olsen, S., et al. (2015). The genomic landscape of juvenile myelomonocytic leukemia. Nat. Genet. *47*, 1326–1333. https://doi.org/10.1038/ng.3400.

61. Ghosh, J., Kobayashi, M., Ramdas, B., Chatterjee, A., Ma, P.L., Mali, R.S., Carlesso, N., Liu, Y., Plas, D.R., Chan, R.J., and Kapur, R. (2016). S6K1 regulates hematopoietic stem cell self-renewal and leukemia maintenance. J. Clin. Invest. *126*, 2621–2625. https://doi.org/10.1172/Jci84565.

62. Zhu, F.F., Feng, M.Y., Sinha, R., Seita, J., Mori, Y., and Weissman, I.L. (2018). Screening for genes that regulate the differentiation of human megakaryocytic lineage cells. Proc. Natl. Acad. Sci. U S A *115*, E9308–E9316. https://doi.org/10.1073/pnas.1805434115.